npj | natural hazards

Article

https://doi.org/10.1038/s44304-025-00146-8

Interpretable machine learning incorporating major lithology for regional landslide warning in northern and eastern Guangdong

Wenfeng Cui[1], Kejie Chen[1,2] ✉, Zhanhui Qing[2,3], Zhiwen Zheng[2,3], Wei Zhang[2,3], Zhihua Zhou[2,3], Peng Han[1], Junling Zhang[4], Zhaoyu Zhu[4] & Chuangeng Sun[1]

Landslides pose major risks in northern and eastern Guangdong, China, due to complex geology and heavy rainfall. Traditional models often oversimplify lithology and lack interpretability. This study develops a lithology-specific random forest model that distinguishes between sedimentary and igneous rocks and integrates rainfall, geological, and geotechnical data. Using 754 landslide cases and 1233 rainfall records, the model achieves over 90% hit rate and below 4% false alarm rate. Interpretable machine learning techniques, including feature importance rankings, SHAP values, and partial dependence plots, are used to understand how different factors contribute to landslide occurrence. A case study from the 2024 Pingyuan landslides confirms the model's real-world applicability. This framework offers improved prediction performance and interpretability and can serve as a robust tool for regional early warning and risk management in geologically diverse areas.

Landslides, those occurring in mountainous regions, pose severe threats to human life and infrastructure worldwide[1]. In regions like northern and eastern Guangdong, China, a complex interplay of geological and climatic factors heightens this risk[2]. Here, intricate granitic landscapes, combined with the subtropical monsoon climate, create conditions that are especially prone to slope failures. Intense rainfall events, such as those during the "Dragon-boat Rain" period[3], further exacerbate landslide susceptibility, underscoring the urgent need for effective risk assessment and mitigation strategies. Historical incidents have repeatedly demonstrated the vulnerability of these landscapes to rainfall-induced landslides, reinforcing the importance of refined, data-driven predictive frameworks[4].

Conventional approaches to landslide prediction include physically based models, empirical rainfall thresholds, and statistical learning methods. Physically based models[5–8] simulate hydrological and geotechnical processes controlling slope stability, but their data and calibration requirements often limit large-scale application. Empirical or statistical models, such as those based on rainfall intensity-duration thresholds[9–14], have been widely adopted due to their simplicity and lower data demand, yet they typically assume uniform geological conditions and neglect lithological variability. While these methods have provided valuable insights, their applicability in geologically diverse regions like Guangdong remains limited. Such models rarely account for the nuanced geological and geotechnical characteristics of the terrain. For example, the intricate properties of granite residual soils—prevalent in the study area—are often oversimplified, reducing the reliability of predictions[15,16]. Furthermore, the lack of attention to model validation and uncertainty quantification further limits the reliability of many traditional methods[17,18]. These challenges hinder the effectiveness of traditional methods, as they struggle to capture the dynamic interactions between varied lithologies, complex geological structures, and fluctuating climatic conditions.

Recent advances in machine learning (ML) techniques offer promising alternatives to these conventional approaches[19–22]. By integrating diverse datasets—ranging from lithological and geological information to meteorological patterns and historical landslide records—ML-based models can identify complex, non-linear relationships and yield more accurate, site-specific predictions. Algorithms such as logistic regression, random forest, and neural networks have successfully improved the performance of landslide prediction or warning, demonstrating their capability to incorporate multiple influencing factors into cohesive predictive frameworks[23–26]. This paradigm shift is particularly relevant in regions like northern and eastern

[1]Department of Earth and Space Sciences, Southern University of Science and Technology, Shenzhen, China. [2]South China Field Scientific Observation and Research Station for Climate-Driven Landslide Risk, Ministry of Natural Resources, Guangzhou, China. [3]Guangdong Geological Environment Monitoring Station, Guangzhou, China. [4]Guangzhou Institute of Geochemistry, Chinese Academy of Sciences, Guangzhou, China. ✉e-mail: chenkj@sustech.edu.cn

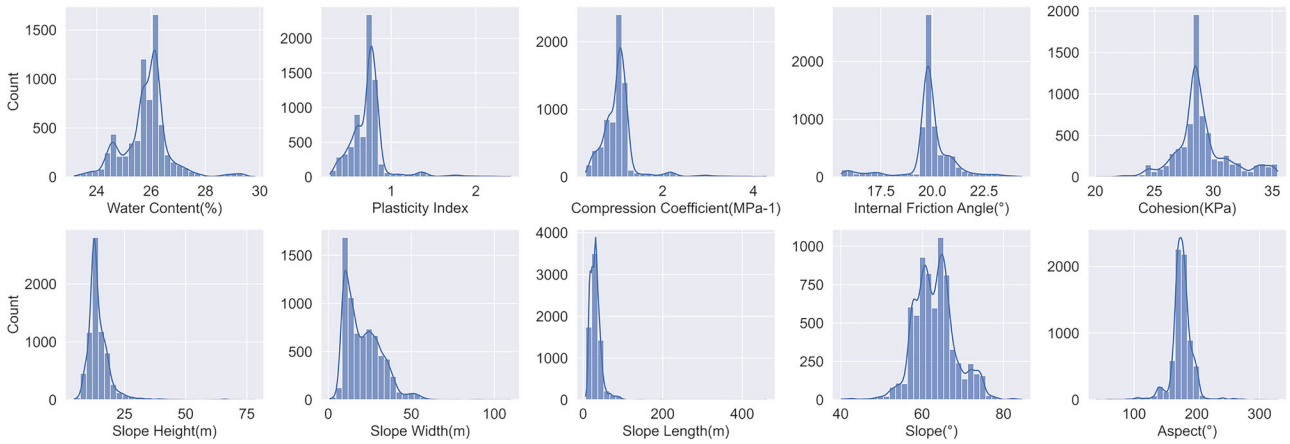

Fig. 1 | Feature distribution across the dataset. Histogram plots show the frequency distribution of each non-rainfall feature across all samples.

Guangdong, where the geological conditions demand more sophisticated analytical methods.

Despite these advancements, many ML approaches still oversimplify lithology, typically treating it as a single input feature. This abstraction fails to capture the distinct responses of various lithological types to infiltration, weathering, shear stresses, and other geomechanical processes[27]. A one-size-fits-all model overlooks the subtle but critical differences between rock types and their evolving responses to environmental triggers, undermining predictive accuracy and limiting the utility of such models in heterogeneous landscapes.

Another significant challenge in current machine learning applications is the issue of black-box models, which offer limited interpretability. These models often operate as opaque systems that provide little insight into the reasoning behind their predictions[28], particularly when models may conflate main controls with secondary environmental variables. This lack of transparency complicates model validation, debugging, and trust-building, especially in domains where understanding the relationship between input features and outcomes is crucial, such as geomechanics and environmental sciences. Therefore, achieving a balance between high predictive performance and interpretability remains a key hurdle in the development of machine learning models that can be effectively applied to complex, real-world problems[29]. Techniques such as SHAP (SHapley Additive exPlanations) and Partial Dependence Plots (PDP) offer partial solutions by quantifying feature impacts and visualizing variable interactions[30–32].

In this context, our study employs a Random Forest (RF) algorithm to improve landslide early warning capabilities for northern and eastern Guangdong. We focus on two predominant lithologies—igneous and sedimentary rocks—to account for their unique mechanical and hydrological behaviors. By incorporating detailed lithological information, geological environment factors, geotechnical properties, rainfall data, and historical landslide records, our approach selects the RF model from various machine learning methods for its ability to handle complex, non-linear data relationships. Moreover, explainable artificial intelligence such as feature importance analysis, SHAP and PDP were embedded into the RF model. Through this interpretable lithology-specific modeling, we aim to enhance both the accuracy and reliability of short-term landslide predictions, providing a more nuanced understanding of landslide mechanisms and offering valuable insights for improved geohazard management in geologically diverse regions.

Results

Exploratory data analysis

The data analysis focuses on investigating the statistical distributions and relationships of geotechnical and geological parameters with lithology to establish its significance as an independent factor in modeling.

To examine the data comprehensively, we began by analyzing the distribution of each feature (Fig. 1). Histograms revealed that most features exhibit unimodal distributions, although their symmetry and spread vary. For example, features such as water content and internal friction angle demonstrate near-symmetric distributions, suggesting quasi-normal behavior. However, certain parameters, including compression coefficient and slope length, exhibit pronounced skewness, indicating potential non-linear relationships or the presence of outliers. This variability highlights the need for more advanced approaches to ensure robust modeling.

The distributions of each feature under two major lithologies are shown in Fig. 2. A comparative analysis of these distributions highlights significant variability in geotechnical properties and geological metrics between igneous and sedimentary lithologies. To quantify lithology-dependent contrasts, we applied two-sample Wilcoxon rank-sum tests (for medians) and Student's t-tests (for means) to each non-rainfall feature, comparing igneous and sedimentary groups. These formal tests yielded large test statistics with p-values < 0.05 for all features (most $\ll 0.001$), supporting that the differences observed in Fig. 2 are statistically significant and reflect robust lithological effects rather than random variation.

Sedimentary rocks exhibit higher water content due to secondary porosity from fractures and weathering, which enhances their permeability and water retention. Their lower compression coefficient and cohesion are linked to weaker cementation and a more granular structure, leading to lower shear strength and compressive resistance[33]. In contrast, igneous rocks typically have lower water content, not only due to their dense crystalline structure but also because of fewer fractures, although weathering can create void spaces that affect permeability. The data also show higher plasticity index and internal friction angle, reflecting the strong interlocking of mineral crystals in granitic rocks, which enhances their mechanical strength and resistance to deformation[34]. These findings also suggest the reason why sedimentary rock landslides are more frequent than igneous rock events.

Slope geometry further reflects lithological influences, with sedimentary formations associated with longer, more confined slopes and igneous formations forming steeper, broader slopes due to differences in material strength and erosion resistance. Aspect distributions, however, appear less affected by lithology, likely influenced more by regional tectonics or climate. These findings underline the necessity of using lithology as an additional prerequisite to differentiate models. By accounting for the specific mechanical behaviors and morphological patterns associated with each lithology, such models can more accurately capture the interactions between material properties and failure mechanisms.

To assess the independence and interrelationship of the features, we assumed all variables follow independent continuous Gaussian distributions and then calculated Pearson correlation coefficients for each pair of features (Fig. 3). Pearson correlation measures the strength and direction of linear relationships between variables, with values ranging from −1 (perfect negative

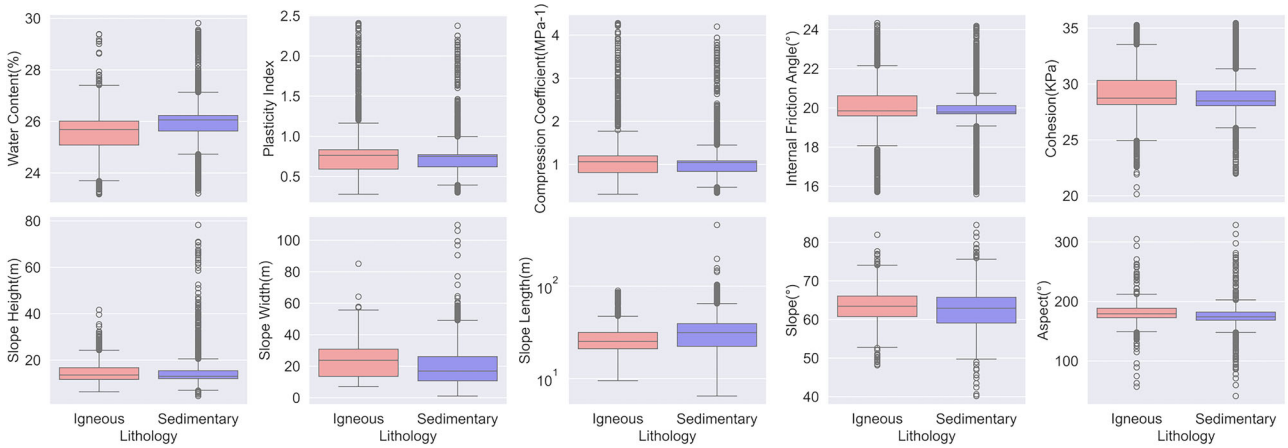

Fig. 2 | Feature variability by lithology type. Box plots display the distribution of each non-rainfall feature, grouped by lithology type (igneous and sedimentary). Boxes represent interquartile ranges, horizontal lines indicate medians, whiskers extend to 1.5× the interquartile range, and points denote outliers.

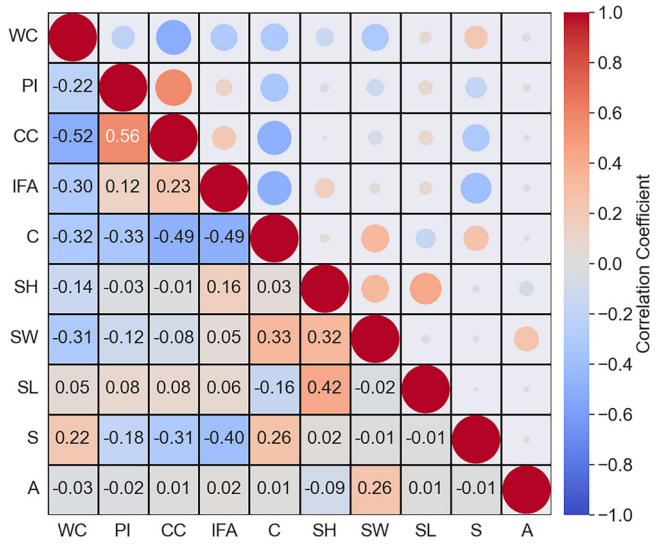

Fig. 3 | Correlation matrix of feature pairs. WC water content, PI plasticity index, CC compression coefficient, IFA internal friction angle, C cohesion, SH slope height, SW slope width, SL slope length, S slope, A aspect.

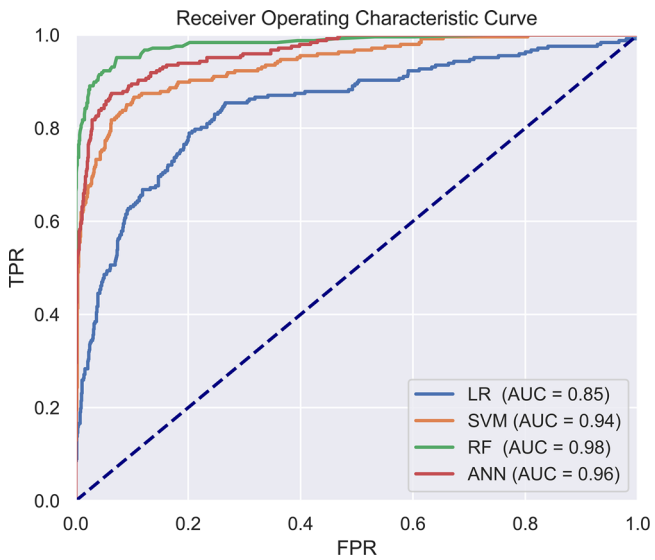

Fig. 4 | ROC curves of machine-learning models. ROC curves compare the performance of the four machine-learning models on the testing set. The area under each curve (AUC) quantifies predictive skill.

correlation) to 1 (perfect positive correlation). The results indicated that most features exhibited weak correlations (absolute values below 0.3), while a few pairs showed moderate correlations (absolute values between 0.3 and 0.5).

We also calculated the variance Inflation Factor (VIF) for each input variable to ensure the independence of the predictors. VIF is a statistical measure used to assess the degree of multicollinearity in regression models. As a rule of thumb, a VIF value greater than 10 suggests significant multicollinearity. We found that all variables had a VIF value below 10, indicating that multicollinearity is not a significant issue in our work. While some moderate multicollinearity ($5 < VIF < 10$) was detected among certain features, such as slope and water content, this is expected in terrain modeling and does not compromise the model's validity or performance, especially given the robustness of tree-based algorithms. The findings suggest that these features can be considered independent, providing a robust foundation for subsequent modeling and offering insights into potential mechanisms underlying landslide occurrences.

Comparison of machine learning models

To select the most appropriate method for our landslide prediction model, we compared multiple ML models, including Logistic Regression (LR), Support Vector Machine (SVM), Random Forest (RF), and Artificial Neural Network (ANN). Here, we adopt a broad definition of ML, under which LR is included as a baseline classifier for binary prediction tasks. At this stage, lithology was not differentiated but treated as a categorical feature encoded into the dataset for training. Since some models require data normalization, we applied Z-score standardization to ensure all features were on a comparable scale.

We use the ROC curve to evaluate the models' performance (Fig. 4). The RF model outperformed all others with an AUC of 0.98, indicating its superior performance. The ANN model followed closely behind, with the SVM model showing competitive results as well. However, the LR model performed the weakest across all metrics. This outcome suggests that while LR is simple and easy to use, it struggles with more complex problems compared to advanced algorithms. The RF model's robust handling of complex data and high-dimensional features makes it the most suitable choice for this task. Given the promising results of SVM and ANN, these models could also be useful for highly demanding classification tasks, but based on our comparison, we chose RF to enhance the accuracy and reliability of landslide early warning predictions.

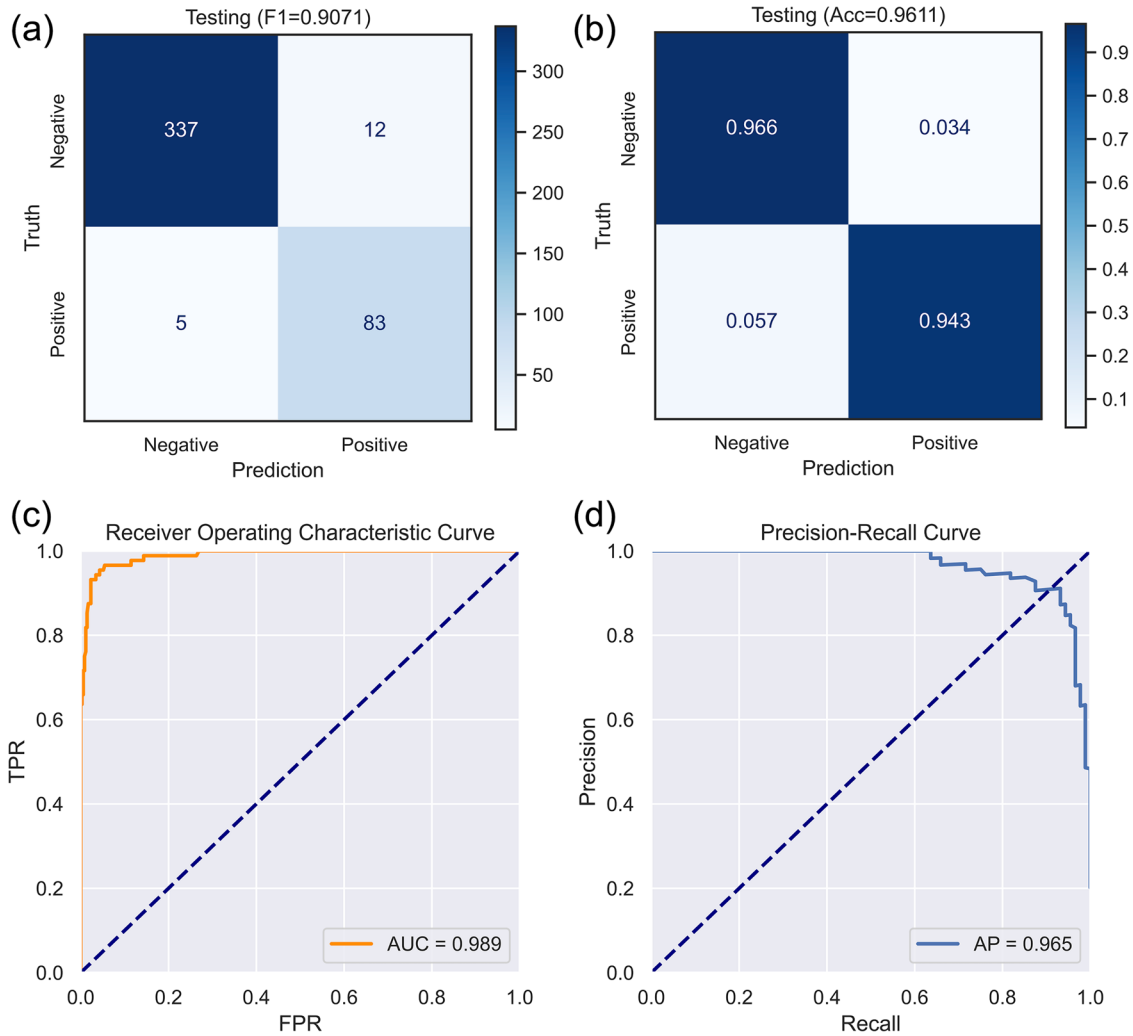

Fig. 5 | Numerical and graphical evaluations of the igneous model. a The confusion matrixes. **b** The confusion matrixes normalized over the true conditions. Accuracies are displayed on the title, with the bottom-right element representing the hit rate, the bottom-left element representing the miss rate, and the top-right element representing the false alarm rate. **c**, **d** ROC curve and PR curve.

Model training and results

For igneous lithology, we randomly divided the dataset of 2184 entries into an 80% training set and a 20% testing set. Utilizing the Bayesian optimization algorithm combined with ten-fold cross-validation, we determined the optimal set of hyperparameters. The default output threshold for the RF classifier is set at 0.5. Considering the specific policies of our study area, it is prudent to issue warnings and take preventive measures when the relative probability of a landslide occurring exceeds 0.4. Therefore, we adjusted the threshold to 0.4 to match the threshold specified by the warning center. This adjustment means that when the model predicts the probability of an event occurring to be over 0.4, it is classified as a positive instance (indicating a prediction of occurrence). Conversely, predictions falling below this threshold are considered negative instances (indicating a prediction of non-occurrence). This adjustment enhances the model's relevance and responsiveness to the specific risk tolerance and safety requirements of the study area.

The efficacy of the RF model in predicting landslides based on an integrated analysis of precipitation, geological environment, and geotechnical mechanics features is underscored by the confusion matrix (Fig. 5a). This matrix visualizes the predictive accuracy of machine learning models, clearly depicting their performance in classifying events correctly. Based on the confusion matrix, we derived several key numerical metrics (Fig. 5b). On the testing dataset, the model achieved a f1 score of 0.9071, an accuracy of 96.11%, a hit rate of 94.3%, a miss rate of 5.7%, and a false alarm rate of only 3.4%. This indicates that the model performs well, with only three misses and four false alarms in numerical terms.

In addition to the confusion matrix, the Receiver Operating Characteristic (ROC) curve (Fig. 5c) and the Precision-Recall (PR) curve (Fig. 5d) provide further insights into the model's predictive capabilities. With an Area Under the ROC Curve (AUC) of 0.989 and an Average Precision (AP) of 0.965, the model demonstrates excellent generalization ability. In summary, the model has been well-trained and exhibits robust performance.

For sedimentary lithology, we also randomly divided the dataset of 4899 entries into an 80% training set and a 20% testing set. Using the same approach, we determined the optimal set of hyperparameters. On the testing dataset, the model achieved a f1 score of 0.9114, an accuracy of 97.14%, a hit rate of 90.6%, a miss rate of 9.4%, and a false alarm rate of 1.6%, resulting in only three missed and twelve false alarms numerically. Additionally, the model performed well with an AUC of 0.992 and an AP of 0.974 (Fig. 6). Both models, for igneous and sedimentary lithologies, demonstrated satisfactory performance, indicating their readiness for practical application in landslide prediction and early warning systems.

Global Interpretability of RF model

The Random Forest (RF) algorithm includes a built-in feature importance measure[35], which quantifies the contribution of each feature to the model's predictive power. This measure ranks predictive variables based on their usefulness in making accurate predictions, thereby providing valuable

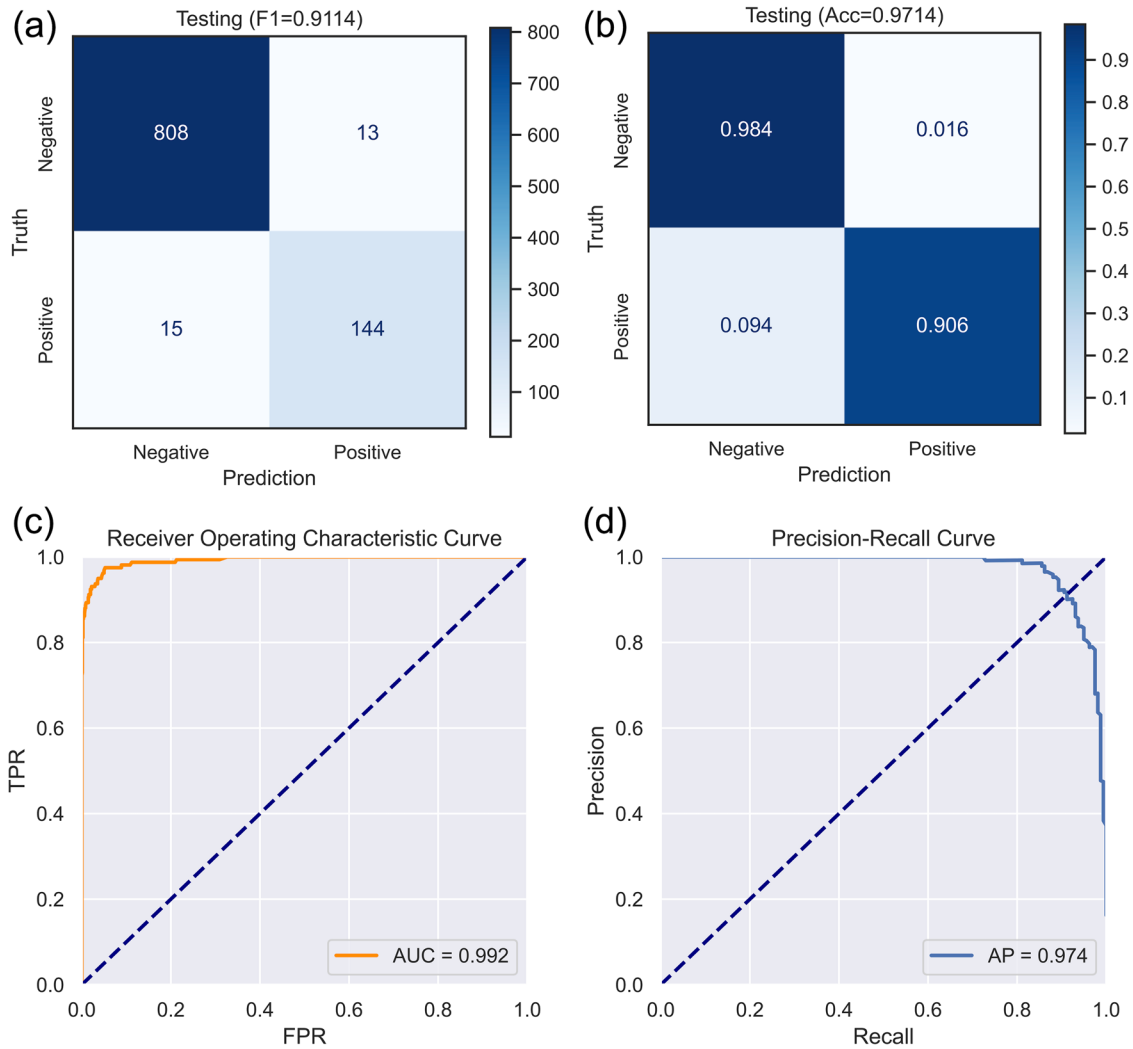

Fig. 6 | Numerical and graphical evaluations of the sedimentary model. Format same as the igneous results in Fig. 5.

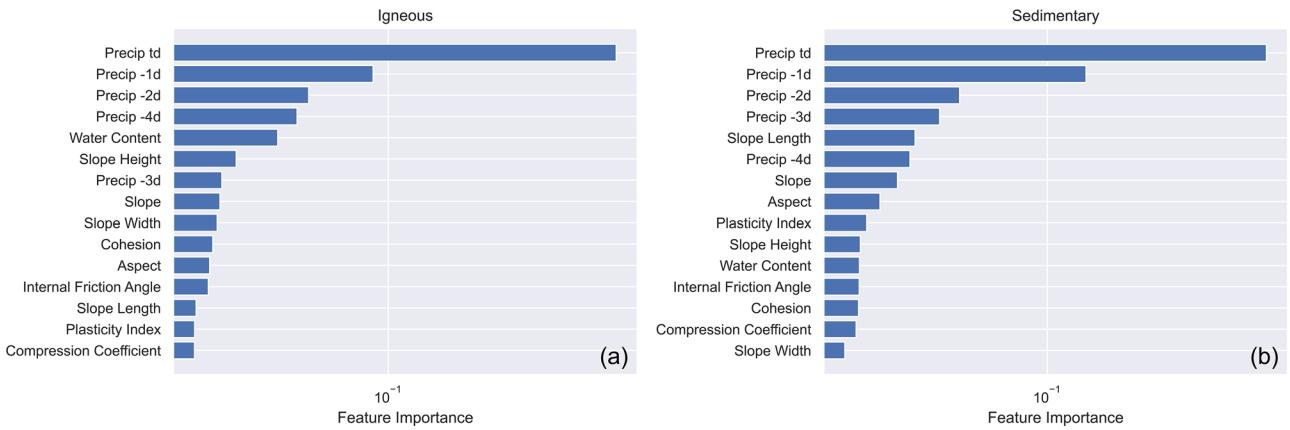

Fig. 7 | RF features importance by lithology. a Rankings for igneous lithology. **b** Rankings for sedimentary lithology. Bar length indicates the relative contribution of each feature to model predictions.

insights into the key factors contributing to landslides (see Fig. 7). This global explanation helps to understand the overall contribution of each feature across all predictions. Feature importance is calculated based on the decrease in impurity caused by each feature across all trees in the forest. Features that result in larger decreases in impurity are considered more important. This metric not only aids in understanding the model but also in feature selection and optimization by highlighting which features are most influential in predicting the target output.

SHAP also provides a similar feature importance ranking through the use of summary beeswarm plots (Fig. 8). These plots offer an intuitive visualization of how each feature contributes to the model's predictions. In a beeswarm plot, the horizontal axis represents the SHAP values of each

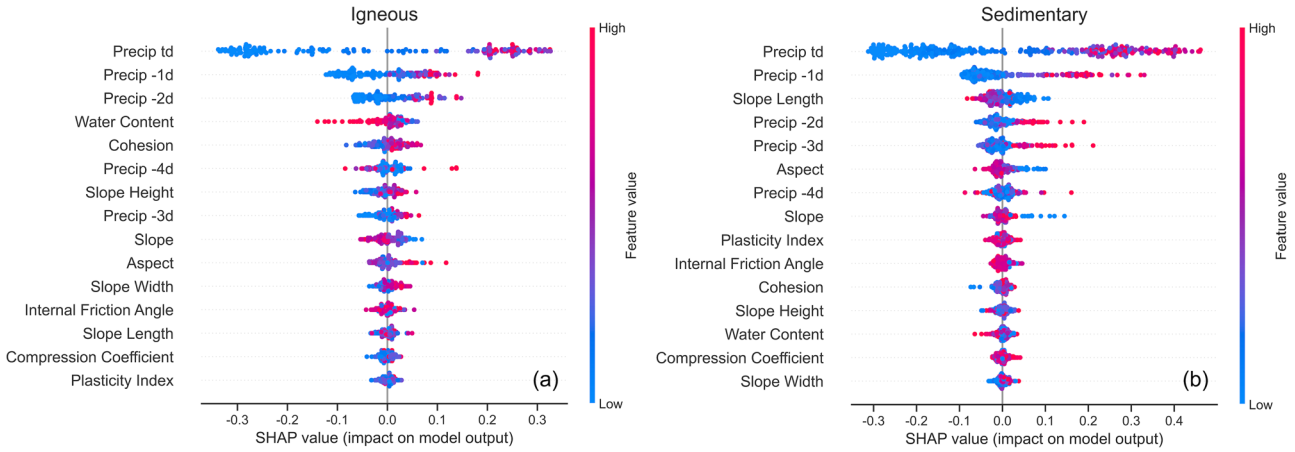

Fig. 8 | SHAP summary beeswarm plots. a Igneous lithology and **b** sedimentary lithology on testing set. Each point represents a SHAP value for a single prediction, colored by the feature value (blue = low, red = high), summarizing overall feature influence.

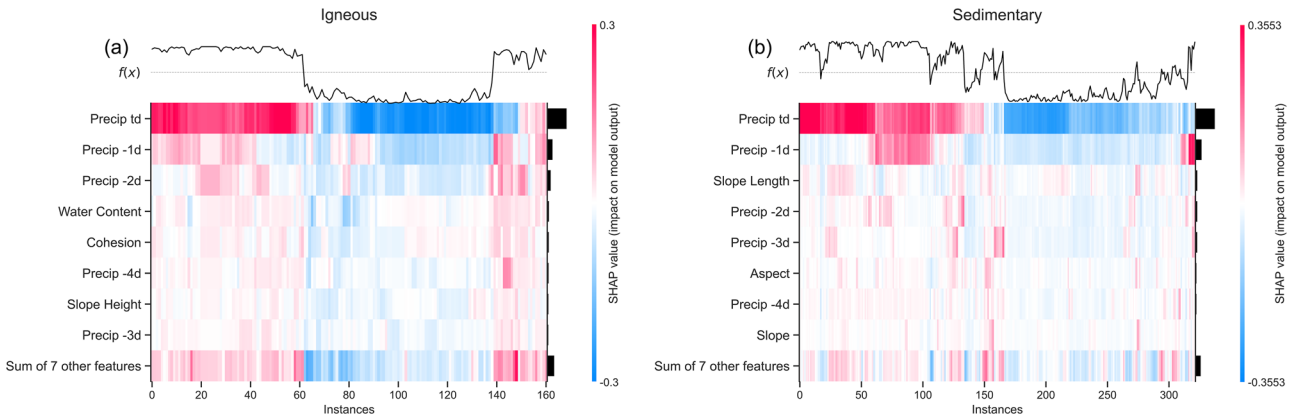

Fig. 9 | SHAP decision heatmaps. a Igneous lithology and **b** sedimentary lithology on testing set. Heatmaps display SHAP values across samples (rows) and features (columns), where color intensity indicates positive or negative contributions to predicted probability.

sample for the corresponding feature. A SHAP value greater than 0 indicates that the feature has a positive contribution to predicting a landslide, while a SHAP value less than 0 suggests a negative contribution to the prediction. The color encoding in the plot indicates the feature value, with colors ranging from low to high values, providing insight into how the magnitude of the feature value influences the prediction. This visualization helps to identify not only which features are important but also how their specific values affect the model's predictions in different samples.

The discrepancy between the feature importance rankings in Fig. 7 (RF model) and Fig. 8 (SHAP analysis) arises from the different mechanisms used by these two techniques. RF importance provides a global view of feature significance based on overall model performance, while SHAP values offer a local, instance-level explanation, revealing how individual feature values contribute to specific predictions. Despite slight differences in the ranking, the most important 8 to 10 features identified by both methods are largely consistent, reflecting a similar overall mechanism. The use of SHAP for generating PDPs in the next section was specifically chosen because it provides a more detailed, localized understanding of feature contributions, which is crucial for interpreting the varying influence of features under different conditions.

SHAP decision heatmaps are another powerful global explanation tool that helps visualize the relationship between feature contributions and model predictions across the entire dataset (Fig. 9). In a SHAP decision heatmap, the horizontal axis represents the test set samples for landslide data after hierarchical clustering, grouping similar samples together. The color encoding indicates the magnitude of the SHAP values for each feature, with warmer colors representing higher SHAP values and cooler colors indicating lower contributions. The vertical axis displays the various features, while the baseline, denoted as f(x), represents the model's default prediction before considering the specific feature contributions. If the resulting output curve is above the baseline, the model predicts a landslide, otherwise the model predicts non-landslide.

The heatmap shows how each feature's contribution varies across the testing set, with warmer colors indicating higher contributions to landslide prediction. The figure highlights the importance of specific features, such as precipitation and geotechnical factors, and shows how these features interact with one another in influencing the model's output. While precipitation is a dominant factor in predicting landslide occurrences, non-precipitation factors serve as important modifiers that can adjust the risk levels based on the unique characteristics of the terrain, geotechnical properties, and slope conditions. This will highlight the complexity of the model and the interplay between various factors influencing landslide predictions.

Precipitation factors unsurprisingly emerged as the most influential features in our model, with rainfall on the day of the event being significantly more important than other variables. The combined importance of precipitation features over a three-day span account for more than half of the total importance. This underscores the dominance of rainfall in triggering landslides in the studied region. However, it is equally important to note that non-precipitation factors also played a crucial supportive role. These factors were able to significantly adjust the influence of precipitation in certain cases, correcting for situations where the rainfalls alone overstated or understated the landslide risk.

Sedimentary rocks typically exhibit higher porosity and permeability compared to igneous rocks, making them highly susceptible to infiltration during rainfall events. This infiltration can elevate pore water pressure and significantly reduce effective stress, leading to a decrease in shear strength and eventual slope failure[36]. Moreover, the sensitivity of sedimentary rocks to precipitation can be linked to their composition, which often includes clay-rich materials prone to swelling and softening under wet conditions[37].

In contrast, igneous rock landslides show a slightly lower cumulative importance for precipitation factors. The relatively low porosity and higher intact strength of igneous rocks diminish the direct influence of rainfall on slope stability. Instead, precipitation's effect is more indirect, such as through increased slope weight or localized saturation zones. Nevertheless, rainfall continues to play a significant role in igneous rock landslides. We propose that the higher degree of weathering observed in the igneous rocks within the study area have enhanced their sensitivity to rainfall, resulting in a greater vulnerability to precipitation-induced instability than would typically be observed in less weathered, more intact igneous materials[38].

The mechanical stability of igneous slopes is predominantly governed by their strength and structural integrity. Water content is particularly influential, as localized saturation can weaken discrete planes of weakness or fault zones[39]. Additionally, terrain attributes such as slope height and aspect directly affect the gravitational driving forces, making them critical in high-steep terrain typically associated with igneous rocks. The role of internal friction angle and cohesion further reflects the strength-dependent nature of igneous rock landslides, where failure occurs primarily through structural or planar mechanisms. The relatively stable structure of igneous rocks contributes to the confidence and stability of model predictions. This structural consistency results in less variability in the model's output, as the predictable nature of the mechanical properties in igneous slopes reduces uncertainty in landslide susceptibility.

For sedimentary rocks, slope length, in particular, is a key factor as it determines the extent of water infiltration and accumulation along the slope, which can destabilize the material over time. The plasticity index's high importance is indicative of the clay-rich composition of many sedimentary rocks, which exhibit significant shear strength reduction when wet. The compression coefficient reflects the compressibility of sedimentary materials under loading or wetting, further contributing to slope failure. These factors collectively suggest that sedimentary landslides are strongly influenced by hydrological processes and material properties that control their response to water.

These findings reveal distinct landslide mechanisms in our study region: igneous rock landslides are predominantly terrain- and strength-controlled, with failure modes involving structural instability, while sedimentary rock landslides are more water-driven, with mechanisms influenced by hydrological processes and material weakening.

Local Interpretability from features

To further interpret the model, we perform local Interpretability at the feature levels. The three most influential non-precipitation features will be focused on using PDP, which illustrate the relationship between each feature and landslide occurrence, as well as their interactions.

For igneous model, the three key features are water content, cohesion, and slope height. A decrease in water content below 26% is associated with a marked increase in landslide dependency, suggesting that low water content increases the material's apparent cohesion. Higher cohesion (above 29 KPa) and increased slope height (above 12 meters) are linked to a significantly higher likelihood of landslides, as shown in Fig. 10. These results highlight the importance of the degree of weathering in the igneous rocks of the study area. The higher apparent cohesion in weathered igneous rocks, which is primarily due to matrix suction or weak cementation, can appear substantial under dry conditions but significantly decreases upon wetting or disturbance, making the slope more susceptible to failure. Additionally, the combination of slope height and cohesion plays a critical role in the landslide risk, especially when the material's strength is reduced or the slope is very steep[40].

The sedimentary rock PDP reveals a different set of relationships (Fig. 11). The key features here are slope length, aspect, and slope. Slope length and aspect are both negatively correlated with landslide dependency. Specifically, when slope length exceeds ~25 meters, the aspect of the slope becomes the dominant factor influencing landslide risk. Aspect is primarily determined by the terrain's orientation, which governs water drainage and sun exposure—two factors that significantly affect slope stability. Slope angle also plays a crucial role in landslide prediction with relatively high dependency throughout the entire range. For steep slopes, the risk of failure increases a bit due to potential sliding along bedding planes or jointed structures, where the potential slip surface is less steep than the slope itself, facilitating sliding. For gentler slopes, the risk slightly increases due to the formation of perched water tables on low-permeability layers, which leads to an increase in pore pressure and material weakening. This can result in translational sliding along weak or residual failure surfaces, contributing to the observed landslide dependency[41].

These findings clearly demonstrate that non-precipitation features have a greater influence on landslide prediction in igneous rocks than in sedimentary rocks. This further underscores the idea that igneous rock slopes exhibit a lower dependency on precipitation compared to sedimentary rock slopes, highlighting the distinct behaviors of these two rock types in landslide susceptibility.

Graded warning model performance comparison

Since 2003, China has progressively implemented regional landslide meteorological warning services, achieving notable success in disaster prevention and mitigation[42]. In alignment with the *Technical Guidelines for Meteorological Risk Early Warning of Geological Hazards at the Municipal Level in Guangdong Province*, we classify the landslide warning probabilities based on model predictions. For an output probability $P \le 20\%$, no warning is issued (indicated as a gray warning); for $P > 20\%$ and $P \le 40\%$, a blue warning is issued; for $P > 40\%$ and $P \le 60\%$, a yellow warning is dispatched; for $P > 60\%$ and $P \le 80\%$, an orange warning is released; and for $P > 80\%$, a red warning is proclaimed, signaling the highest level of alert.

To demonstrate the advantages of our approach, we compared it with two traditional statistical models: the implicit statistical warning model and the explicit statistical warning model. The implicit model categorizes precipitation into different ranges by calculating early effective precipitation amounts:

$$R_p = kR_1 + k^2R_2 + \ldots + k^nR_n \quad (1)$$

where R_p is the amount of precipitation that impacts landslides during the precipitation process prior to their occurrence, R_n is the daily precipitation on the nth day before, n is the number of effective precipitation days, and k is the effective precipitation coefficient set to 0.84. Corresponding warnings are issued based on the range within which the precipitation falls[43]. Building on this, the explicit model incorporates geological environmental factors and employs Principal Component Analysis (PCA) to extract main components that account for a total contribution rate of 90%. It calculates a potentiality score for each landslide point[44,45]. These scores, combined with effective precipitation, are then used to delineate warning levels:

$$T = G * (R_d + R_p) \quad (2)$$

where G is the potentiality score from geological environment, R_d is the daily precipitation on the day of the landslide occurrence, and R_p is the early effective precipitation amount.

In evaluating our model's effectiveness, we conducted a comprehensive comparison across the testing dataset against traditional statistical methods, which utilize all landslide points for analysis. To facilitate a nuanced examination, tests were conducted separately on positive and negative cases across different lithologies, calculating hit rates and false alarm rates for each. It is noteworthy that blue warnings, typically issued online without subsequent action, are classified as non-landslide indicators in our analysis. The results (see Fig. 12) reveal that our RF model significantly outperforms

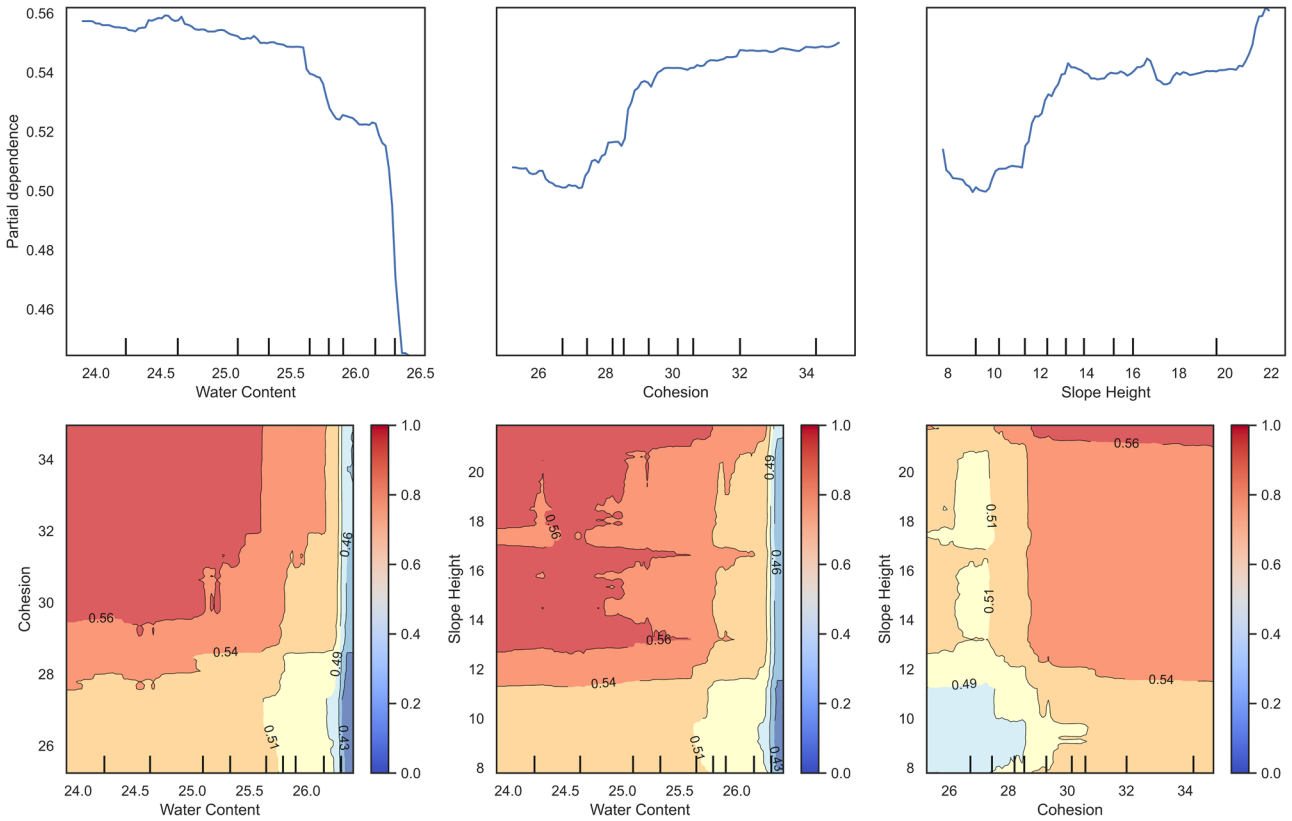

Fig. 10 | Igneous PDPs of the most important three non-precipitation features. Top are relationships between features and landslide probability. Bottom are synergistic effects of features on landslide probability. Color bar on the right represents the probability predicted by the RF model.

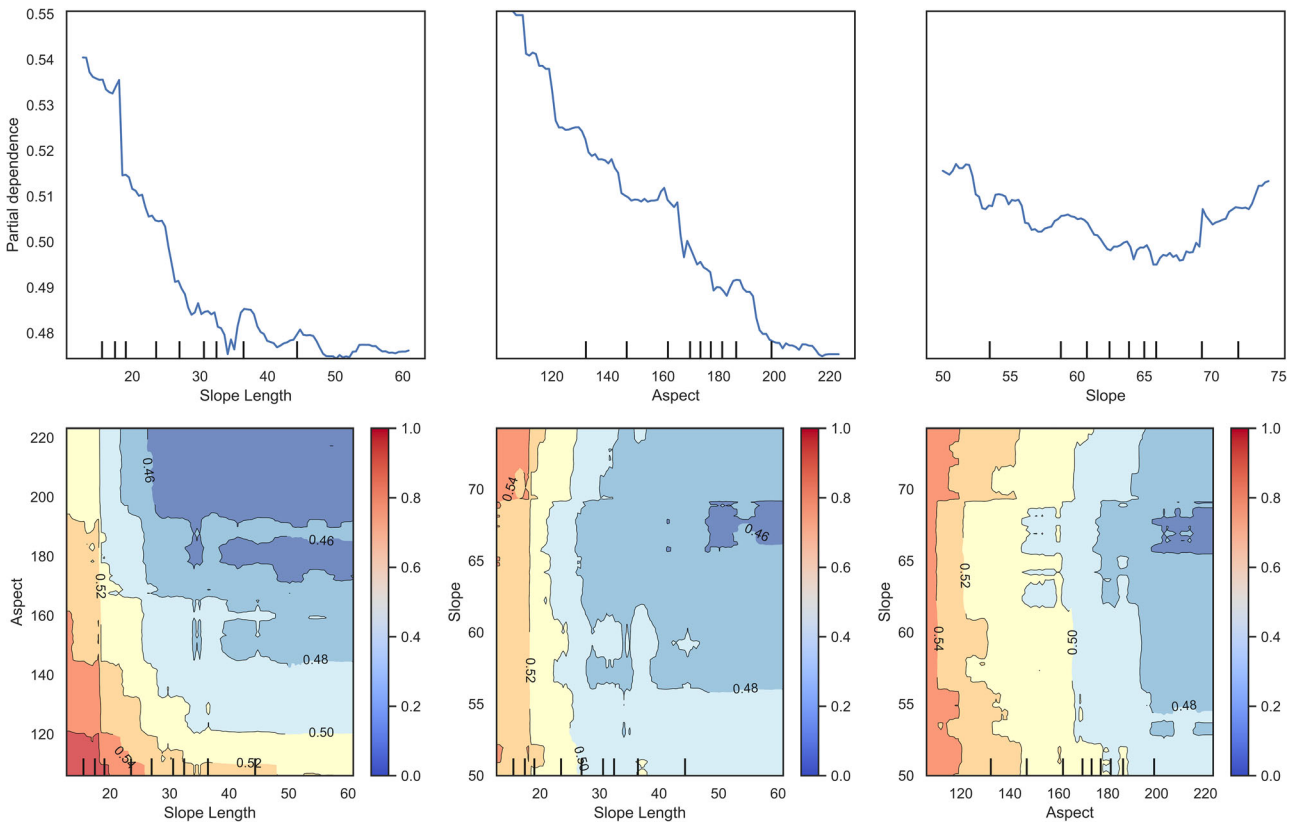

Fig. 11 | Sedimentary PDPs of the most important three non-precipitation features. Format same as the igneous PDPs in Fig. 10.

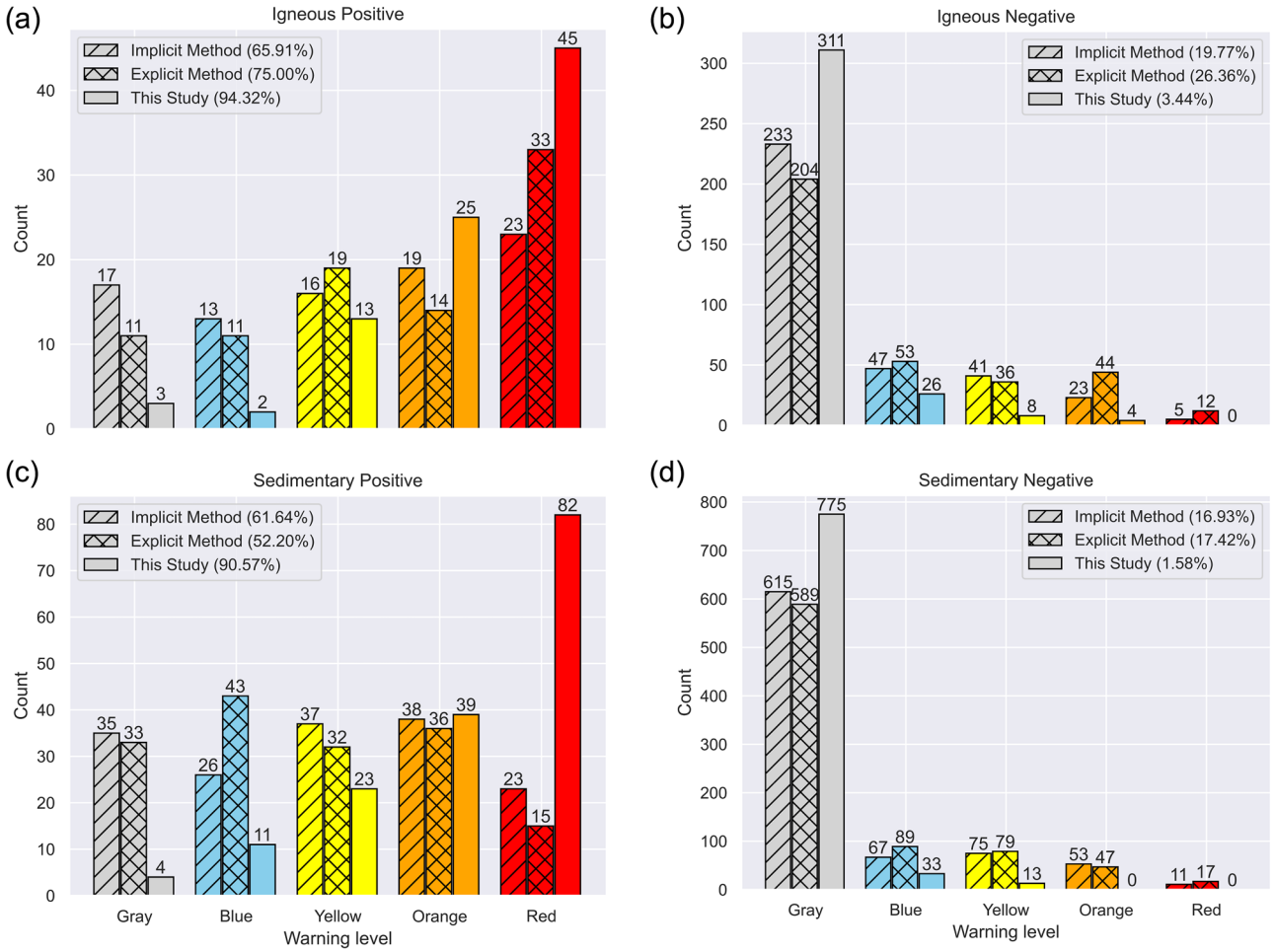

Fig. 12 | Comparison of graded warning performance between RF model used in this study, implicit statistical model, and explicit statistical model. a Results on positive samples of igneous lithology, with hit rates in the legend. **b** Results on negative samples of igneous lithology, with false alarm rates in the legend. **c**, **d** Same as (**a**) and (**b**) but for sedimentary lithology.

the traditional statistical models in both igneous and sedimentary rock regions, delivering higher hit rates (94.32% and 90.57%) and lower false alarm rates (3.44% and 1.58%). Furthermore, the accuracy in tier classification is markedly improved; for positive cases, our model predominantly issues red or orange warnings, indicative of an imminent landslide. Conversely, for negative cases, it almost exclusively issues gray or blue warnings, denoting a negligible risk of occurrence.

Application on rainfall-induced landslides in Pingyuan County in June 2024

Pingyuan County, located in northeastern Guangdong, China, experienced severe rainfall-induced landslides on June 16, 2024. This event led to significant fatalities and economic losses, with rainfall reaching up to 360 mm in a single day. The region's steep terrain, granite lithology, and prolonged rainfall contributed to the widespread slope failures, highlighting the vulnerability of the area to monsoon-driven landslides[46].

Pingyuan County is situated within our study area, and there are three available rainfall gauge stations in the region (Fig. 13a). For this application, we utilized daily rainfall data from June 1 to June 16, 2024, from these stations. Using the corresponding lithology-based RF model, we conducted landslide predictions for this period by a 5-day window to assess the practical feasibility of our method in a real-world setting. The model issued daily warnings from June 5, confirming its potential to predict landslides and assist in early disaster prevention.

During the period leading up to the landslides, when rainfall had not yet reached extreme levels, the model did show a small number of false alarms (Fig. 13b). These occurred due to slight increases in rainfall on the days when the 5-day sliding window was updated. However, it is important to note that these false alarms were all within the yellow warning level, meaning they were relatively low-risk predictions and were quickly corrected as the rainfall data progressed.

On June 16, as rainfall levels surged, all three stations issued warnings at or above the orange level, which closely aligned with the significant increase in precipitation on that day. Notably, the final warning levels and probability values varied across the stations, and upon closer examination, we found that these differences corresponded well with the number of landslides within the warning zone of each station. This suggests that the model was effectively accounting for both the intensity of the rainfall and the local topographic factors, enhancing its ability to provide tailored and reliable early warnings for landslides. This case study serves as a validation of our approach and demonstrates its applicability in real-world landslide forecasting.

Discussion

In order to assess the effectiveness of the lithology-based model construction and the incorporation of geotechnical parameters—factors typically not considered separately or included in traditional methods—a series of comparative experiments were conducted under four distinct scenarios:

1. Without distinguishing lithology and without geotechnical parameters.
2. Without distinguishing lithology but including geotechnical parameters.
3. Distinguishing lithology but without geotechnical parameters.
4. Distinguishing lithology and including geotechnical parameters.

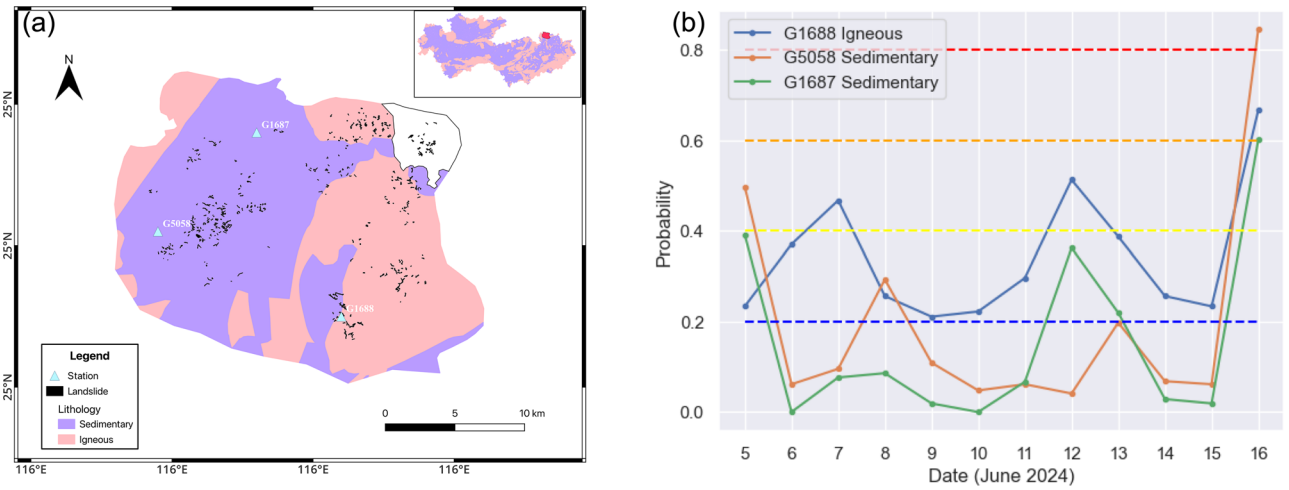

Fig. 13 | Application in Pingyuan. a Lithology, rainfall stations, and landslide distribution in Pingyuan County (upper right corner indicates the county's location within the study area). **b** Daily landslide warning probabilities for the three rainfall stations from June 1 to June 16, 2024, based on the sliding 5-day window. The blue, orange, and green lines represent the Igneous (G1688) and Sedimentary (G5058, G1687) lithologies, respectively, with color-coded thresholds marking landslide warning probabilities.

Table 1 | Performance metrics for different model configurations

Condition	Accuracy	F1-Score	Hit rate	Miss rate	False alarm rate
1	93.79%	0.81	77.3%	22.7%	2.7%
2	94.78%	0.85	81.8%	18.2%	**2.5%**
3	94.88%	0.86	85.4%	14.6%	2.7%
4	**96.63%**	**0.91**	**92.45%**	**7.55%**	**2.5%**

Bold values represent the best performance.

The same data preprocessing and feature selection methods were applied across all scenarios to ensure fair comparison, and the models that distinguishes lithology will take the average of the performance metrics for comparison. Scenarios 1 and 3 excluded geotechnical parameters, while scenarios 2 and 4 included them. Additionally, scenarios 1 and 2 did not account for distinguishing lithology, with the models trained and tested on the entire dataset and with lithology as one of the input features. Scenarios 3 and 4, however, constructed and tested models based on specific lithological types (igneous and sedimentary rocks), respectively. The consolidated performance metrics for each scenario are presented in Table 1.

The results of these experiments indicate that incorporating geotechnical parameters enhances model performance, with marked increases in accuracy and decreases in false alarm rate, regardless of lithology distinction. This underscores the critical importance of geotechnical data in accurately predicting landslides. Models that differentiate lithology demonstrate superior performance compared to those that do not, achieving higher accuracy and lower false alarm rate. The most effective model configuration is achieved when both lithology and geotechnical parameters are included, resulting in the highest accuracy, f1 score and hit rate, and the lowest miss and false alarm rates, as shown in the final configuration of Table 1.

These findings validate the approach of integrating lithology and geotechnical parameters in the model. This comprehensive method significantly enhances the accuracy and reliability of landslide prediction, offering valuable insights for early warning systems and risk mitigation strategies in geologically diverse regions.

To further interpret the model, we perform local Interpretability at sample levels. We create two individual waterfall plots for a landslide and a non-landslide case (Fig. 14). These plots clearly illustrate how the model independently predicts each sample and the impact of each feature on the target variable. The two cases are particularly insightful because they highlight situations where precipitation features give misleading predictions, and non-precipitation features step in to correct the model's output. This further emphasizes the important role of geological and geotechnical parameters in refining the model's predictions.

The use of rain gauge stations as the primary source for precipitation data presents notable limitations in landslide warning systems. The spatial resolution of this data is inherently low, making it challenging to pinpoint the exact locations of potential landslides. This limitation significantly affects the system's ability to provide localized early warnings, as the heterogeneity of rainfall distribution within a region cannot be accurately captured[47]. Additionally, the temporal resolution of the data, often constrained to daily measurements, impedes the system's capability to issue precise warnings on an hourly basis. The uncertainty surrounding the exact timing of landslides complicates timely intervention. To address these limitations, the integration of satellite meteorological data offers a promising alternative[48]. Satellite data can provide higher spatial and temporal resolution, enabling more accurate assessments of precipitation patterns over specific areas of interest. Adopting such data could substantially enhance the system's predictive accuracy, allowing for more timely and localized warnings.

Accurately determining geological and geotechnical factors for landslides is challenging due to reliance on interpolation methods to fill data gaps. While these methods are invaluable for creating continuous surfaces from discrete points, they inherently assume that environmental properties change smoothly across space. This assumption can lead to significant inaccuracies in areas where geological features exhibit abrupt changes, such as fault lines or regions with varied rock types[49]. The interpolated data may not accurately represent the complex geological conditions that critically influence landslide susceptibility. One potential improvement involves integrating high-resolution geospatial data, such as LiDAR (Light Detection and Ranging) and InSAR (Interferometric Synthetic Aperture Radar) imagery[50,51]. These technologies can provide detailed topographical and geological information, offering insights into surface deformations, slope stability, and rock layer orientations. Additionally, advancements in geostatistical methods, such as kriging with external drift[52] or machine learning-based interpolation techniques[53], could offer more nuanced approaches to modeling geological variability. Implementing these technologies and methods would enhance the spatial accuracy of geological and geotechnical factors, thereby improving the early warning system's predictive capacity.

Additionally, this study's analysis was constrained by data availability, prompting the simplification of lithological diversity into two broad categories. While this approach supported a more robust model due to improved data balance, it also overlooked the finer-scale variability inherent in specific rock types. Different lithologies can exhibit substantial differences

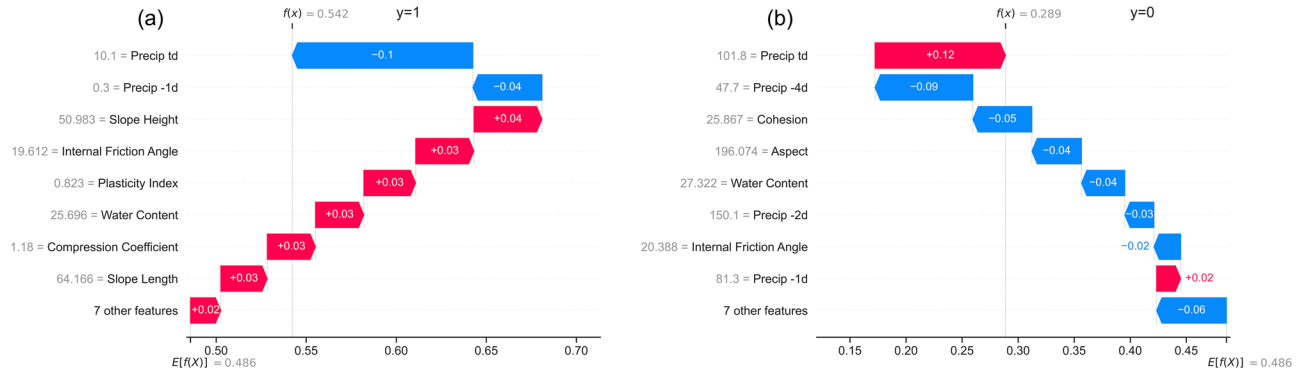

Fig. 14 | SHAP waterfall plots for representative samples. a Landslide sample and **b** non-landslide sample. The y-axis of is the feature value, the x-axis is the SHAP value, E[f(x)] presents the expectation of all sales, and f(x) represents the predicted probability.

in geotechnical properties, influencing the mechanical and hydrological behavior of the derived soils. Future efforts should aim to collect more extensive and detailed datasets, ultimately enabling the development of more finely tuned, lithology-specific models. Such models would better capture the subtle variations in rock and soil properties, improving our understanding of landslide processes and enhancing the precision of landslide prediction and mitigation strategies.

While the proposed method shows promise for landslide early warning, there are several limitations that need to be addressed for improved practical application in real-world scenarios. One key limitation is the current definition of rainfall events, which is based on a fixed 5-day window and may not fully capture the dynamic nature of rainfall-triggered landslides. Future improvements could involve adopting more advanced, objective methods for defining rainfall events, potentially incorporating real-time rainfall thresholds and dynamic models that account for spatial and temporal variations[14]. Additionally, integrating weather forecast data into the model could significantly enhance its predictive capabilities by providing more accurate earlier warnings, particularly in rapidly changing weather conditions. Another avenue for improvement is the integration of landslide susceptibility maps[54–56], which could be used to assess the reliability of the warnings by considering the spatial distribution of landslides. This combined approach would not only improve the model's accuracy but also help prioritize areas with higher susceptibility, making the early warning system more targeted and effective for disaster mitigation. Based on both empirical evidence and data limitations, tectonic processes, seismic activity, and variations in rock mass quality were not explicitly incorporated into the analysis, assuming that the study area is relatively tectonically stable, seismically inactive, and exhibits uniformly high rock mass quality[57,58]. However, these factors could still play an important role in landslide susceptibility[59,60]. Future research that incorporates detailed fracture characteristics, tectonic activity, and seismic factors, along with lithology and geotechnical properties, could enhance the robustness of landslide hazard predictions.

Building on the above findings, this study demonstrates the potential of a machine learning-based approach—specifically, a RF model—to enhance landslide prediction in northern and eastern Guangdong. By integrating a broad spectrum of data sources, including rainfall records, geological factors, and geotechnical properties, we achieved significant improvements in prediction accuracy and reduced false alarms compared to conventional statistical methods. A notable advancement lies in moving beyond lithology-agnostic models to incorporate geological and geotechnical variability. While this study simplified lithological categories into two main types (igneous and sedimentary), this step acknowledges the critical influence of lithology on landslide behavior.

In addition to improving performance, the use of interpretability tools such as feature importance rankings, SHAP values, and partial dependence plots helped clarify the underlying mechanisms driving predictions. These insights improve model transparency and facilitate better understanding of how both precipitation and non-precipitation factors contribute to landslide occurrence, strengthening stakeholder trust in model outputs.

Future research, supported by more detailed lithological data, can further refine this approach. Nonetheless, the proposed lithology-informed framework already offers substantial benefits for regional landslide early warning systems and provides a practical foundation for more targeted disaster risk reduction strategies.

Methods

Study area

The study area spans the northern and eastern regions of Guangdong Province, China, including the cities of Qingyuan, Shaoguan, Heyuan, and Meizhou (Fig. 15). Geologically, this area is characterized by widespread distributions of both igneous and sedimentary rocks (Fig. 16a), resulting in a distinctive stratigraphy. At the surface, loose and permeable weathered soils blanket more rigid, less permeable rock strata[61]. These weathered soils contain abundant capillary pores, which promote rainfall infiltration and consequently reduce the shear strength of the soil and underlying rock layers.

The region's stratigraphy can be further categorized to capture its lithological diversity (Fig. 16). Sedimentary rocks comprise four main groups: sandstone and conglomerate, shale and mudstone, carbonate rocks, and red clastic rocks. Similarly, igneous rocks are represented by granite, migmatitic granite, granodiorite, and volcanic clastic rocks. Overlying these bedrock units, colluvial soils—formed through rainfall-induced erosion and downslope sediment transport—accumulate along slope midsections and at slope bases[62]. These colluvial soils contain well-developed pores and fissures, which facilitate rapid infiltration of rainwater and subsequent reductions in soil strength. Such conditions significantly enhance the susceptibility of the area to landslides.

Although multiple subtypes of igneous and sedimentary rocks exist in the study area, the data distribution across these detailed lithologies is highly imbalanced (Fig. 16b). As summarized in Table 2, most individual lithologies lack sufficient event records for robust model training. To address this limitation, we consolidated these subtypes into two broader lithological categories—sedimentary rocks and igneous rocks—for the purpose of model development. This simplification ensures more sufficient datasets and enhances the reliability of the subsequent modeling and analysis.

The topography of our study area is primarily mountainous and hilly, accounting for over 60% of the terrain and characterized by extensive, steep slopes[63]. Slopes exceeding a certain meter in height with gradients above 45° are particularly prone to landslide hazards, a common feature in this region. Such steep slopes, especially those composed of sedimentary rocks, are more susceptible to instability under gravitational forces, significantly increasing the likelihood of landslides and posing a constant threat to the region[64]. The interaction between geomorphological and geological conditions creates a dynamic environment where even minor triggers, such as heavy rainfall, can lead to substantial slope failures and subsequent landslides[65].

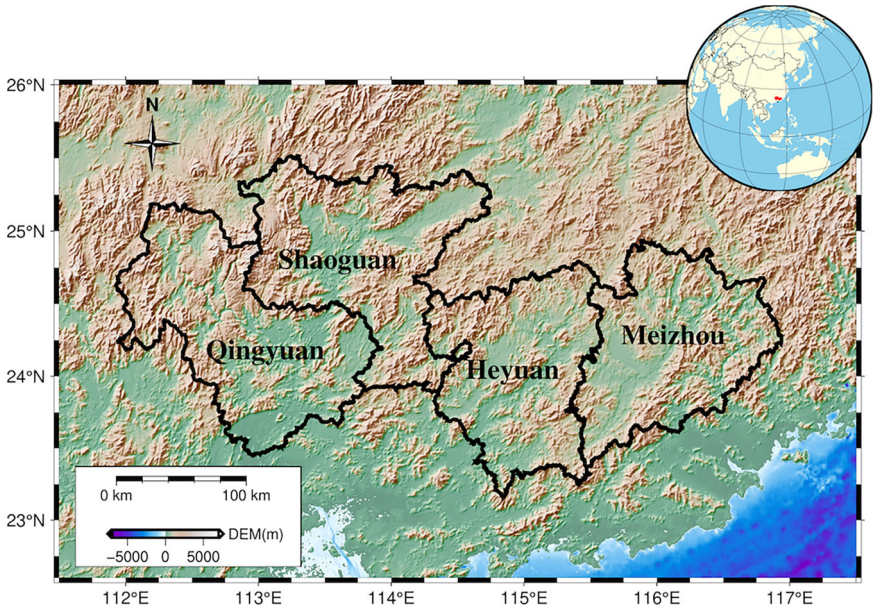

Fig. 15 | Topographic background and administrative division map of the study area. The inset map shows the location of the study area.

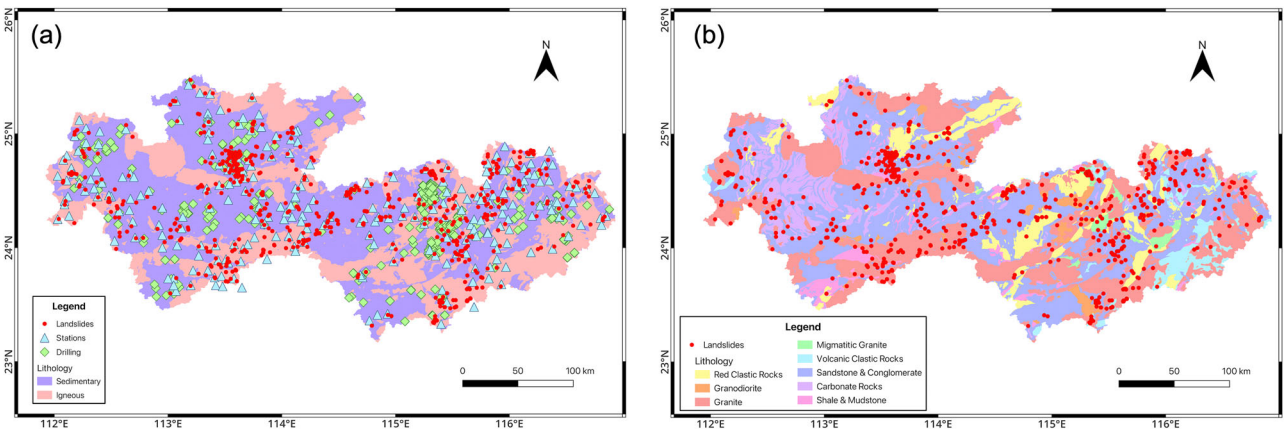

Fig. 16 | Lithology maps. a Landslide inventory in the study area with the rain gauge stations and drilling points. The lithology of the geological background is shown in different colors. **b** Relatively detailed distribution map of geological lithology, with red dots indicating landslide events.

Table 2 | Statistics of landslide event records under various lithologies

Geological categories	Geological subcategories	Quantity
Sedimentary	Red clastic rocks	87
	Sandstone & Conglomerate	605
	Shale & Mudstone	30
	Carbonate rocks	72
Igneous	Granite	322
	Migmatitic granite	68
	Granodiorite	29
	Volcanic clastic rocks	20

Climatically, the region falls within the subtropical humid climate zone, experiencing cold, dry winters and hot, rainy summers. The intense rainfall, particularly during the "Dragon-boat Rain" season from late spring to early summer, synergizes with numerous rivers and abundant groundwater. This combination significantly enhances rainwater penetration, increasing pore water pressure in soils and rocks, impacting the geological environment, and heightening the risk of landslides[66]. The combination of heavy rainfall and the hydrogeological context creates conditions conducive to soil saturation and slope instability[67]. Together, these factors exacerbate the likelihood of landslides (Fig. 17), posing a significant threat to the region's safety and infrastructure.

Data preprocessing

Our dataset compiles rainfall-induced landslides—most of which are classified as earth slides—with relatively accurate records of onset times in the study area from 2013 to 2022. The occurrence of these landslides results from a complex interplay among rainfall conditions, geological environments, and geotechnical parameters. While traditional warning models often only consider these factors in isolation, our approach integrates them to enable a more comprehensive analysis.

Rainfall has been widely recognized as the primary trigger for most landslides in the study area. Rainfall data were collected from rain gauge stations located within a 10 km radius of each landslide site. Given the limited temporal resolution of the landslide occurrence records, we analyzed daily rainfall data and considered the cumulative precipitation for each of the five days preceding each event. This approach accounts for the effect of antecedent rainfall and yields five separate rainfall-related features. The five-day window represents a compromise between practical experience and the time frames commonly adopted by local monitoring

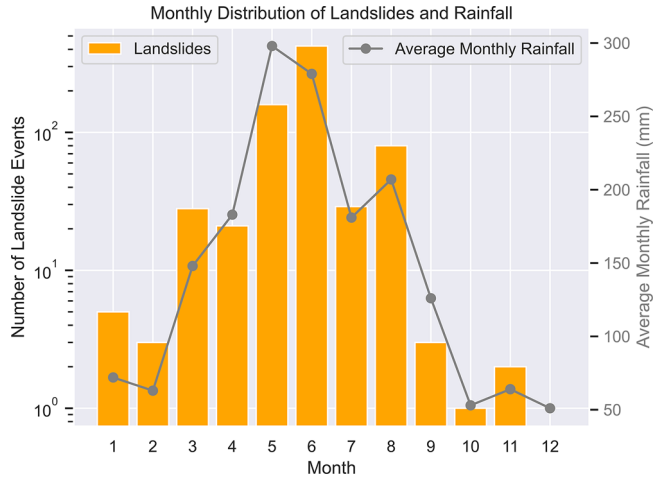

Fig. 17 | Relationship between the number of landslides and their occurrence months in our study area from 2013 to 2022. The annual average monthly rainfall data is sourced from the yearbooks of the four cities in 2023, which reflect the average rainfall for the past ten years (2013–2022).

agencies[68,69], ensuring consistency in model inputs for ML-based landslide warning systems.

Geological environment data describes the background conditions of the sample points, encompassing six features: slope height, slope width, slope length, slope, aspect, and lithology. Geotechnical parameters, derived from 1386 drilling points in the study area, include five features: water content, plasticity index, compression coefficient, internal friction angle, and cohesion, which are a set of key parameters selected to reduce high correlation and extract the most representative parameters for landslide prediction, which are both independent and can comprehensively reflect the mechanical and hydrological characteristics of soil. In this study, "rock" is used as a general term to represent bedrock lithology, but under strong weathering these rocks often degrade into saprolite or colluvium layer and behave more like soils, which justifies the use of geotechnical parameters such as the plasticity index.

Crucially, landslide warning is treated as a binary classification problem, with outputs labeled as occurrence (1) or non-occurrence (0). Our dataset contains both positive (landslide points) and negative (non-landslide points) samples. Positive samples were selected from a historical inventory, requiring precise spatial and temporal coordinates and proximity (within 10 km) to a rain gauge station. Following these criteria, we identified 754 landslide events between May 2013 and November 2022. For each event, data from up to three nearby rain gauges provided daily precipitation for the preceding five days.

We then spatially overlaid these positive samples with the geological and geotechnical data (Fig. 16a) to extract relevant features. For point-distributed attributes like drilling data, we used local weighted regression interpolation for different lithologies to estimate values at landslide locations.

Data cleaning was a crucial part of the dataset construction process. We removed positive samples where the five-day precipitation preceding the landslide was nearly zero, as this was inconsistent with the known rainfall-triggering patterns. Since the landslide inventory explicitly records rainfall as a trigger, such cases were potentially caused by instrument malfunctions or localized events. Additionally, we manually corrected anomalies in the geological and geotechnical data: obvious recording errors, such as missing decimal points or exceeding valid limits, will be corrected or removed. This rigorous cleaning process yielded a final set of 1233 high-quality positive records, providing a robust foundation for analysis and model development.

We define negative samples as points where no landslides occurred. Since these points are not directly available and precipitation is a primary trigger for landslides, we derived negative samples through random sampling, using positive samples and rain gauge stations as references while applying specific spatial-temporal constraints.

For spatial sampling, we refined a technique commonly used in geological hazard risk assessment[70,71]. Specifically, we created 10 km buffer zones around each rain gauge station associated with positive samples. Within these buffer zones, we randomly sampled five points per buffer zone to serve as negative samples, which reflects a tradeoff between the limitation of rainfall data and the inherent class imbalance. Any samples that fell outside the study area were discarded, resulting in a total of 5850 negative samples with an approximate 1:5 ratio of positive to negative samples (Fig. 18). Geological and geotechnical features were obtained through spatial overlay analysis, consistent with the process used for positive samples.

Then for temporal sampling, due to the confidentiality and availability of the complete rainfall data, we used a 5-day window to slide over the 9 days of rainfall data prior to the landslide event, obtaining approximately five times the amount of negative sample rainfall data. This approach simulates the daily continuous monitoring of rainfall leading up to a landslide event and enables the issuance of a warning on the day of the event. While this method inevitably introduces some correlation with the landslide, Fig. 19 shows that the negative samples exhibit a good degree of coverage and diversity. This helps ensure significant variability among the negative samples, which aligns with real-world scenarios.

Random Forest model

The Random Forest (RF) algorithm is a versatile machine learning technique[72] whose performance surpasses several other machine learning algorithms. This approach effectively mitigates overfitting, a common limitation of single decision trees, by aggregating diverse predictions from multiple trees, each developed from a random subset of training data and features[73,74]. This ensemble method enhances the model's robustness and accuracy, making it well-suited for complex geological phenomena.

Feature selection is crucial for accuracy of RF. We utilized Bayesian optimization[75] for efficient hyperparameter tuning. This method incrementally refines hyperparameters: n_estimators, max_depth, and min_samples_split—to optimize the RF model's performance. In evaluating the performance of our binary classification RF model, we adopt a multi-faceted set of metrics to comprehensively capture the model's predictive capabilities.

Accuracy is defined as the proportion of true predictions (both positives and negatives) out of all predictions:

$$Acc = \frac{TP + TN}{TP + TN + FP + FN} \tag{3}$$

where TP denotes true positives (correctly predicted occurrences), TN represents true negatives (correctly predicted non-occurrences), FP denotes false positives (predicted occurrences that did not occur), FN represents false negatives (predicted non-occurrences that did occur). Although intuitive, accuracy may not always reflect the model's performance accurately in unbalanced settings. Therefore, we delve deeper into the model's predictive efficiency through the hit rate (or recall), which measures the model's ability to correctly identify actual positives, and the miss rate (false negative rate, FNR), indicating the proportion of positives missed by the model. Furthermore, the false alarm rate quantifies the ratio of incorrectly predicted positives among the actual negatives, helping to assess the model's precision:

$$hit\ rate = \frac{TP}{TP + FN} \tag{4}$$

$$miss\ rate = \frac{FN}{TP + FN} = 1 - hit\ rate \tag{5}$$

$$false\ alarm\ rate = \frac{FP}{FP + TN} \tag{6}$$

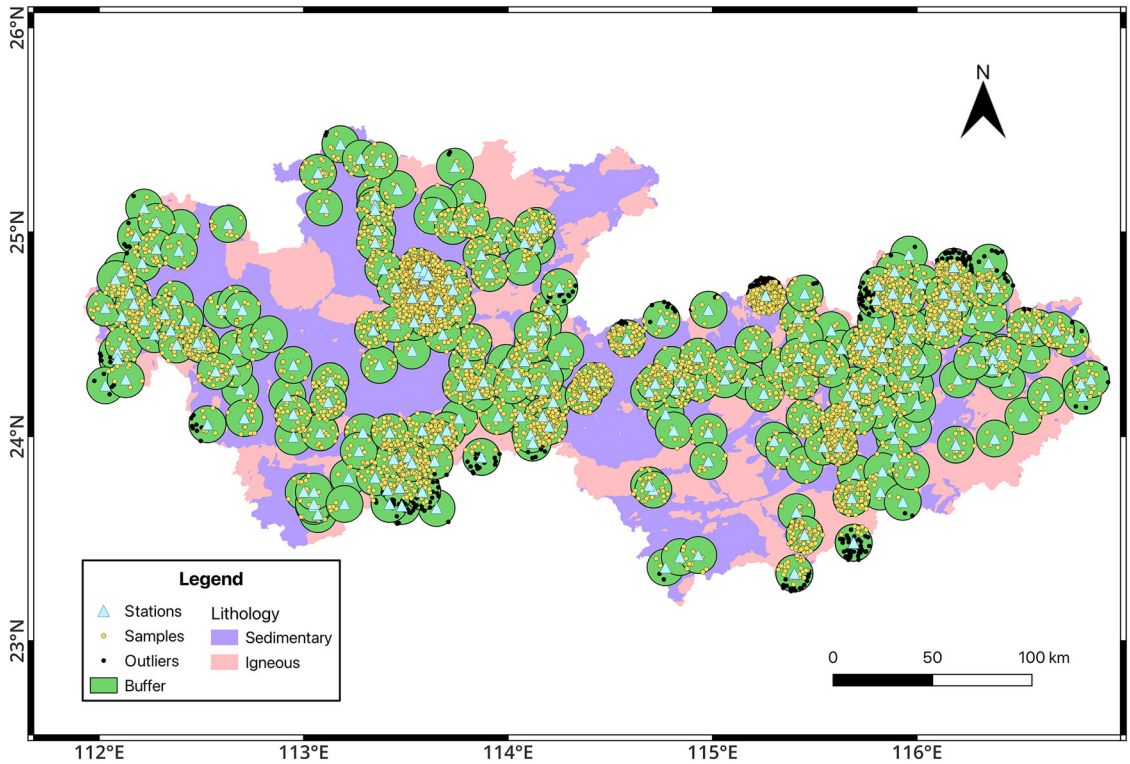

Fig. 18 | The sampling result of negative samples. The blue triangles represent the rain gauge stations, the green circles represent the 10 km buffer zones generated by the rain gauge stations, the yellow dots represent randomly sampled non-landslide points within the study area, and the black dots represent sampling points outside the study area.

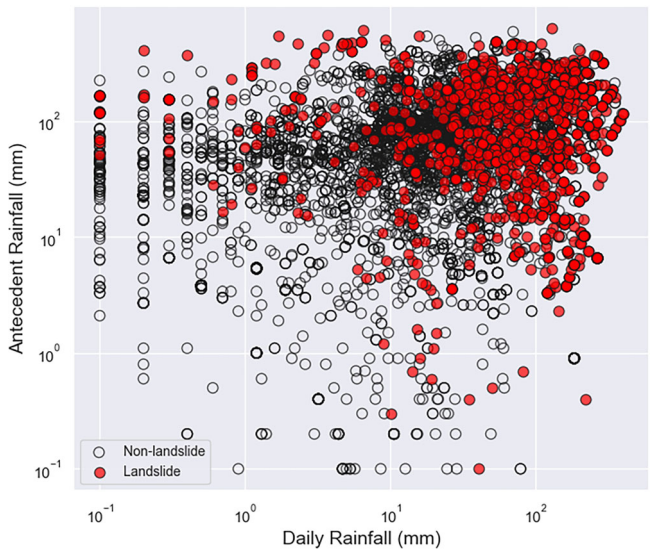

Fig. 19 | Antecedent-daily rainfall distributions for landslide classification. Charts show the relationship between antecedent rainfall and daily rainfall for landslide (red) and non-landslide (hollow black) samples, illustrating the distribution of different rainfall types across events.

Additionally, to offer a more balanced evaluation of the model's performance, we include the F1-Score, which is the harmonic mean of precision and recall. The F1-Score is particularly useful in unbalanced datasets, as it gives a more comprehensive view of the model's ability to both identify true positives and avoid false positives:

$$F1 - Score = \frac{2 \times Precision \times Recall}{Precision + Recall} \quad (7)$$

where Recall is the same as hit rate and Precision is the ratio of true positives to all predicted positives:

$$Precision = \frac{TP}{TP + FP} \quad (8)$$

The Receiver Operating Characteristic (ROC) curve, which plots the true positive rate (TPR, or sensitivity) against the false positive rate (FPR, or 1-specificity), and the area under this curve (AUC) serve as primary indicators of model performance across all possible classification thresholds[76]. The AUC value, where a higher score indicates better performance, provides an aggregated measure of the model's ability to discriminate between classes. Additionally, the Precision-Recall (PR) curve, which plots precision against recall, and its corresponding area under the curve (AP), is particularly insightful in the context of imbalanced datasets, offering a focused view on the model's success in identifying the positive class amidst a majority of negative instances. This comprehensive evaluation framework, underpinned by both numerical and graphical analyses, enables a holistic understanding of the model's strengths and limitations, guiding us toward refined predictive applications.

Data availability

Data will be made available upon reasonable request.

Received: 6 May 2025; Accepted: 12 September 2025;
Published online: 26 September 2025

References

1. Fang, R. K., Liu, Y. H. & Huang, Z. Q. A review of the methods of regional landslide hazard assessment based on machine learning. *Chin. J. Geol. Control* **32**, 1–8 (2021).
2. Zhuo, L., Huang, Y. P., Zheng, J., Cao, J. J. & Guo, D. H. Landslide susceptibility mapping in Guangdong Province, China, using random

forest model and considering sample type and balance. *Sustainability* https://doi.org/10.3390/su15119024 (2023).
3. Dong, S. R. et al. Analysis of precipitation anomaly and a failed prediction during the dragon-boat rain period in 2022. *J. Trop. Meteorol.* **29**, 115–127 (2023).
4. Lin, Z. Y. & Liu, A. H. Landslide disaster distribution characteristics and pre-warning measures of Guangdong Province. *Yangtze River* **50**, 90–92 (2019).
5. Terlien, M. T. J. The determination of statistical and deterministic hydrological landslide-triggering thresholds. *Environ. Geol.* **35**, 124–130 (1998).
6. Caine, N. The rainfall intensity - duration control of shallow landslides and debris flows. *Geografiska Annaler: Ser. A, Phys. Geogr.* **62**, 23–27 (2017).
7. Wilson, R. C. & Wieczorek, G. F. Rainfall thresholds for the initiation of debris flows at La Honda, California. *Environ. Eng. Geosci.* **I**, 11–27 (1995).
8. Yu, P. et al. Study on fluid-solid coupling numerical simulation and early warning of weathered granite landslides induced by extreme rainfall. *Sustainability* https://doi.org/10.3390/su151511738 (2023).
9. Segoni, S., Piciullo, L. & Gariano, S. L. A review of the recent literature on rainfall thresholds for landslide occurrence. *Landslides* **15**, 1483–1501 (2018).
10. Aleotti, P. & Chowdhury, R. Landslide hazard assessment: summary review and new perspectives. *Bull. Eng. Geol. Environ.* **58**, 21–44 (1999).
11. Guzzetti, F., Peruccacci, S., Rossi, M. & Stark, C. P. Rainfall thresholds for the initiation of landslides in central and southern Europe. *Meteorol. Atmos. Phys.* **98**, 239–267 (2007).
12. Guzzetti, F., Peruccacci, S., Rossi, M. & Stark, C. P. The rainfall intensity-duration control of shallow landslides and debris flows: an update. *Landslides* **5**, 3–17 (2008).
13. Saito, H., Nakayama, D. & Matsuyama, H. Relationship between the initiation of a shallow landslide and rainfall intensity-duration thresholds in Japan. *Geomorphology* **118**, 167–175 (2010).
14. Dal Seno, N., Evangelista, D., Piccolomini, E. & Berti, M. Comparative analysis of conventional and machine learning techniques for rainfall threshold evaluation under complex geological conditions. *Landslides* **21**, 2893–2911 (2024).
15. Pennington, C., Freeborough, K., Dashwood, C., Dijkstra, T. & Lawrie, K. The National Landslide Database of Great Britain: Acquisition, communication and the role of social media. *Geomorphology* **249**, 44–51 (2015).
16. Ponziani, F., Berni, N., Stelluti, M., Zauri, R. & Tamagnini, C. *Landwarn: An Operative Early Warning System for Landslides Forecasting Based on Rainfall Thresholds and Soil Moisture* (Springer Berlin Heidelberg, 2013).
17. Frattini, P., Crosta, G. & Sosio, R. Approaches for defining thresholds and return periods for rainfall-triggered shallow landslides. *Hydrol. Process* **23**, 1444–1460 (2009).
18. Jaiswal, P. & van Westen, C. J. Estimating temporal probability for landslide initiation along transportation routes based on rainfall thresholds. *Geomorphology* **112**, 96–105 (2009).
19. Li, J. *Landslide Information Extraction and Risk Assessment of High Resolution Imagery in Weizhou town, Wenchuan County*. Chengdu University of Technology (2019).
20. Xue, C. H., Chen, K. J., Tang, H., Lin, C. Q. & Cui, W. F. Using short-interval landslide inventories to build short-term and overall spatial prediction models for earthquake-triggered landslides based on machine learning for the 2018 Lombok earthquake sequence. *Nat. Hazards* **114**, 3575–3595 (2022).
21. Kang, J. et al. Research on machine learning forecasting and early warning model for rainfall-induced landslides in Yunnan province. *Sci. Rep*. https://doi.org/10.1038/s41598-024-64679-0 (2024).
22. Xu, C. & Xue, Z. Applications and challenges of artificial intelligence in the field of disaster prevention, reduction, and relief. *Nat. Hazards Res.* **4**, 169–172 (2024).
23. Kuradusenge, M., Kumaran, S. & Zennaro, M. Rainfall-induced landslide prediction using machine learning models: the case of Ngororero District, Rwanda. *Int. J. Environ. Res. Public Health* https://doi.org/10.3390/ijerph17114147 (2020).
24. Li, Y. C., Liu, Q. Y., Li, X., Gu, T. H. & Zhang, N. Exploring early warning and forecasting of meteorological risk of landslide and rockfall induced by meteorological factors by the approach of machine learning. *Chin. J. Geol. Hazard Control* **32**, 118–123 (2021).
25. Liu, Y. H., Fang, R. K., Su, Y. C. & Xiao, R. H. Machine learning based model for warning of regional landslide disasters. *J. Eng. Geol.* **29**, 116–124 (2021).
26. Nanda, A. M., Lone, F. A. & Ahmed, P. Prediction of rainfall-induced landslide using machine learning models along highway Bandipora to Gurez road, India. *Nat. Hazards* **120**, 6169–6197 (2024).
27. Segoni, S., Pappafico, G., Luti, T. & Catani, F. Landslide susceptibility assessment in complex geological settings: sensitivity to geological information and insights on its parameterization. *Landslides* **17**, 2443–2453 (2020).
28. Rudin, C. Stop explaining black box machine learning models for high stakes decisions and use interpretable models instead. *Nat. Mach. Intell.* **1**, 206–215 (2019).
29. Ribeiro, M. T., Singh, S. & Guestrin, C. "Why should I trust you?" Explaining the predictions of any classifier. In *KDD'16: Proceedings of the 22nd ACM SIGKDD International Conference on Knowledge Discovery and Data Mining*, 1135–1144 (2016).
30. Lundberg, S. M. & Lee, S. I. A unified approach to interpreting model predictions. In *Advances in Neural Information Processing Systems 30 (NIPS 2017)* 30 (2017).
31. Molnar, C., Casalicchio, G. & Bischl, B. Interpretable machine learning —a brief history, state-of-the-art and challenges. *Comm. Com. Inf. Sc.* **1323**, 417–431 (2020).
32. Wen, H. J., Yan, F. Y., Huang, J. H. & Li, Y. J. Interpretable machine learning models and decision-making mechanisms for landslide hazard assessment under different rainfall conditions. *Expert Syst. Appl.* https://doi.org/10.1016/j.eswa.2025.126582 (2025).
33. Cai, X., Zhou, Z. L., Liu, K. W., Du, X. M. & Zang, H. Z. Water-weakening effects on the mechanical behavior of different rock types: phenomena and mechanisms. *Appl. Sci.* https://doi.org/10.3390/app9204450 (2019).
34. Heap, M. J. & Violay, M. E. S. The mechanical behaviour and failure modes of volcanic rocks: a review. *B Volcanol.* https://doi.org/10.1007/s00445-021-01447-2 (2021).
35. Louppe, G. Understanding random forests: from theory to practice. Preprint at https://arxiv.org/abs/1407.7502 (2014).
36. Grotzinger, J. & Jordan, T. H. *Understanding Earth* (Macmillan, 2010).
37. Azhar, M. U. et al. Water-induced softening behavior of clay-rich sandstone in Lanzhou Water Supply Project, China. *J. Rock. Mech. Geotech.* **12**, 557–570 (2020).
38. Alberti, S., Leshchinsky, B., Roering, J., Perkins, J. & Olsen, M. J. Inversions of landslide strength as a proxy for subsurface weathering. *Nat Commun.* https://doi.org/10.1038/s41467-022-33798-5 (2022).
39. Lan, B. et al. Strength characteristics in saturation process and rainfall-induced landslide failure mechanism of granite residual soil. *Front. Earth Sc.* https://doi.org/10.3389/feart.2025.1578923 (2025).
40. Kinde, M., Getahun, E. & Jothimani, M. Geotechnical and slope stability analysis in the landslide-prone area: a case study in Sawla - Laska road sector, Southern Ethiopia. *Sci. Afr.* https://doi.org/10.1016/j.sciaf.2024.e02071 (2024).
41. Lahusen, S. R. & Grant, A. R. R. Complex landslide patterns explained by local intra-unit variability of stratigraphy and structure: Case study

in the Tyee Formation, Oregon, USA. *Eng. Geol.* https://doi.org/10.1016/j.enggeo.2023.107387 (2024).
42. Liu, C. Z., Wen, M. S. & Tang, C. Meteorological early warning of geohazards in China based on raining forecast. *Geol. Bull. China* **23**, 7 (2004).
43. Li, C. J., Ma, T. H. & Zhu, X. S. *Forecasting of Landslides Trigged by Rainfall: Theory, Method and Application* (Geological Publishing House, 2008).
44. Liu, C. Z. et al. Early warning for regional geo-hazards during 2003-2012, China. *Chin. J. Geol. Hazard Control* **26**, 1–8 (2015).
45. Liu, Y. H., Liu, C. Z., Lian, J. F., Wen, M. S. & Tang, C. Method of regional early warning of geohazards based on the explicit statistical theory. *Geol. China* **35**, 344–350 (2008).
46. Zhang, W. et al. Severe rainfall-induced landslides in Pingyuan County, Guangdong, China, in June 2024. *Landslides* https://doi.org/10.1007/s10346-025-02546-3 (2025).
47. Canli, E., Loigge, B. & Glade, T. Spatially distributed rainfall information and its potential for regional landslide early warning systems. *Nat. Hazards* **91**, S103–S127 (2018).
48. Brunetti, M. T., Melillo, M., Peruccacci, S., Ciabatta, L. & Brocca, L. How far are we from the use of satellite rainfall products in landslide forecasting?. *Remote Sens. Environ.* **210**, 65–75 (2018).
49. Wang, Y., Akeju, O. V. & Zhao, T. Y. Interpolation of spatially varying but sparsely measured geo-data: a comparative study. *Eng. Geol.* **231**, 200–217 (2017).
50. He, Y. F. et al. Integration of InSAR and LiDAR technologies for a detailed urban subsidence and hazard assessment in Shenzhen, China. *Remote Sens.* https://doi.org/10.3390/rs13122366 (2021).
51. Xue, C., Chen, K., Tang, H. & Liu, P. Heavy rainfall drives slow-moving landslide in Mazhe Village, Enshi to a catastrophic collapse on 21 July 2020. *Landslides* **19**, 177–186 (2021).
52. Baisad, K., Chutsagulprom, N. & Moonchai, S. A non-linear trend function for kriging with external drift using least squares support vector regression. *Mathematics* https://doi.org/10.3390/math11234799 (2023).
53. Sekulic, A., Kilibarda, M., Heuvelink, G. B. M., Nikolic, M. & Bajat, B. Random forest spatial interpolation. *Remote Sens.* https://doi.org/10.3390/rs12101687 (2020).
54. Obda, I. et al. Landslide susceptibility mapping using GIS Matrix Method and Frequency Ratio, application in the marly context of Moulay Yacoub Region, Morocco. *BSGF-Earth Sci. B* https://doi.org/10.1051/bsgf/2023016 (2024).
55. Sahrane, R. et al. Assessing the reliability of landslides susceptibility models with limited data: impact of geomorphological diversity and technique selection on model performance in Taounate Province, Northern Morocco. *Earth Syst. Environ.* **9**, 421–445 (2025).
56. Ali, M. Z. et al. High-resolution landslide mapping and susceptibility assessment: landslide temporal variations and vegetation recovery. *Adv. Space Res.* **74**, 3668–3690 (2024).
57. Liu, L. B. Stable Continental Region earthquakes in South China. *Pure Appl. Geophys.* **158**, 1583–1611 (2001).
58. Zhou, L. Q. et al. The structure of the crust and uppermost mantle beneath South China from ambient noise and earthquake tomography. *Geophys J. Int.* **189**, 1565–1583 (2012).
59. Brideau, M. A., Yan, M. & Stead, D. The role of tectonic damage and brittle rock fracture in the development of large rock slope failures. *Geomorphology* **103**, 30–49 (2009).
60. Xia, L. et al. Feasibility of coseismic landslide prediction based on GNSS observations: a case study of the 2022 Ms 6.8 Luding, China, Earthquake. *Seismol Res. Lett.* **96**, 244–259 (2025).
61. Peng, P., Wang, C., Wang, X. P. & Yang, S. Y. Qingyuan high-grade granite-greenstone terrain in the Eastern North China Craton: Root of a Neoarchaean arc. *Tectonophysics* **662**, 7–21 (2015).
62. Pang, C. J., Li, Z. X., Xu, Y. G., Wen, S. N. & Krapez, B. Climatic and tectonic controls on Late Triassic to Middle Jurassic sedimentation in northeastern Guangdong Province, South China. *Tectonophysics* **677**, 68–87 (2016).
63. Ma, S. Y., Shao, X. Y. & Xu, C. Characterizing the distribution pattern and a physically based susceptibility assessment of shallow landslides triggered by the 2019 heavy rainfall event in Longchuan County, Guangdong Province, China. *Remote Sens.* https://doi.org/10.3390/rs14174257 (2022).
64. Henriques, C., Zêzere, J. L. & Marques, F. The role of the lithological setting on the landslide pattern and distribution. *Eng. Geol.* **189**, 17–31 (2015).
65. Wu, H. Y., Song, X. D., Liu, F., Li, D. C. & Zhang, G. L. Geophysical and geochemical characterization reveals topography controls on critical zone structure in a low hilly region. *Earth Surf. Proc. Land* **47**, 2796–2810 (2022).
66. Cheng, J. B., Zhao, Y. H., Zhi, R. & Feng, G. L. Meridional circulation dominates the record-breaking "Dragon Boat Water" rainfall over south China in 2022. *Front. Earth Sc.* https://doi.org/10.3389/feart.2022.1032313 (2023).
67. Lü, Q., Wu, J. Y., Liu, Z. H., Liao, Z. X. & Deng, Z. H. The Fuyang shallow landslides triggered by an extreme rainstorm on 22 July 2023 in Zhejiang, China. *Landslides* **21**, 2725–2740 (2024).
68. Deng, R. L. et al. Towards establishing empirical rainfall thresholds for shallow landslides in Guangzhou, Guangdong Province, China. *Water* https://doi.org/10.3390/w14233914 (2022).
69. Xie, C. C. et al. Detailed inventory and initial analysis of landslides triggered by extreme rainfall in the northern Huaiji County, Guangdong Province, China, from June 6 to 9, 2020. *Geoenvironmental Dis.* https://doi.org/10.1186/s40677-025-00311-1 (2025).
70. Xiao, C. C., Tian, Y. A., Shi, W. Z., Guo, Q. H. & Wu, L. A new method of pseudo absence data generation in landslide susceptibility mapping with a case study of Shenzhen. *Sci. China Technol. Sc.* **53**, 75–84 (2010).
71. Yao, X., Tham, L. G. & Dai, F. C. Landslide susceptibility mapping based on Support Vector Machine: a case study on natural slopes of Hong Kong, China. *Geomorphology* **101**, 572–582 (2008).
72. Breiman, L. Random forests. *Mach. Learn* **45**, 5–32 (2001).
73. Kim, J. C., Lee, S., Jung, H. S. & Lee, S. Landslide susceptibility mapping using random forest and boosted tree models in Pyeong-Chang, Korea. *Geocarto Int.* **33**, 1000–1015 (2018).
74. Wang, Y. et al. Optimizing the predictive ability of machine learning methods for landslide susceptibility mapping using SMOTE for Lishui City in Zhejiang Province, China. *Int. J. Environ. Res. Public Health* https://doi.org/10.3390/ijerph16030368 (2019).
75. Snoek, J., Larochelle, H. & Adams, R. P. Practical Bayesian optimization of machine learning algorithms. In *Advances in Neural Information Processing Systems* 4 (2012).
76. Fawcett, T. An introduction to ROC analysis. *Pattern Recogn. Lett.* **27**, 861–874 (2006).

Acknowledgements

The work was funded by the Research Project on Mechanisms of Geological Disasters in Typical Rock Areas (Igneous Rocks and Sedimentary Rocks) in Guangdong Province, China (0835-230Z52801271), and high level special funds (G03050K001). We extend our gratitude to the scikit-learn project for providing the comprehensive machine learning library, which was instrumental in the development and evaluation of our RF models. We thank the developers and contributors of QGIS for providing the powerful and open-source Geographic Information System (GIS) software, which was instrumental in the spatial analysis conducted in this study. QGIS and Python (https://www.python.org) software are used for plotting figures.

Author contributions

W.C. wrote the original draft, developed the methodology, conducted formal analysis, and prepared visualizations. K.C. conceptualized the study, reviewed and edited the manuscript, and secured funding. Z.Q., Z.Zheng,

W.Z., and Z.Zhou managed project administration and conducted investigations. P.H. reviewed and edited the manuscript. J.Z. conducted investigations and secured funding. Z.Zhu and C.S. curated data, reviewed and edited the manuscript. All authors reviewed the manuscript.

Competing interests

The authors declare no competing interests.

Additional information

Correspondence and requests for materials should be addressed to Kejie Chen.

Reprints and permissions information is available at http://www.nature.com/reprints

Publisher's note Springer Nature remains neutral with regard to jurisdictional claims in published maps and institutional affiliations.